Turkish Journal of Electrical Engineering & Computer Sciences

http://journals.tubitak.gov.tr/elektrik/

Research Article

Turk J Elec Eng & Comp Sci
(2017) 25: 1291 – 1299

doi:10.3906/elk-1510-100

A compact wideband printed antenna for free-space radiometric detection of partial discharge

Yong ZHANG[1,*], **Pavlos LAZARIDIS**[1], **Raed ABD-ALHAMEED**[2], **Ian GLOVER**[1]
[1]Department of Engineering & Technology, University of Huddersfield, Huddersfield, UK
[2]School of Electrical Engineering & Computer Science, University of Bradford, Bradford, UK

Received: 14.10.2015 • **Accepted/Published Online:** 26.04.2016 • **Final Version:** 10.04.2017

Abstract: A microstrip line-fed wideband printed antenna is presented for radio detection of partial discharge (PD). The novel simple structure antenna has compact size of 24 × 20 × 0.16 cm^3 (0.28 λ_s× 0.23 λ_s× 0.002 λ_s) and is suitable for radiometric PD wireless sensor nodes, where λ_s is the wavelength of the lowest frequency of the band (i.e. 0.35 GHz). A stepped and beveled radiation patch is used in combination with a slotted ground plane to achieve a wide fractional bandwidth of 119% (0.35 to 1.38 GHz) for a return loss better than 10 dB. Good radiation pattern characteristics are obtained across the frequency band of interest. The match between simulated and experimental results suggests that the design is sound and robust.

Key words: Wideband, compact size, printed antenna, partial discharge, radio detection

1. Introduction

Partial discharge (PD) may occur when a usually earthed metallic component in an item of a high voltage (HV) plant becomes disconnected from the ground. PD monitoring can play a valuable role in the ongoing maintenance of HV plants. The location of PD sources by free-space radio detection is an attractive approach for condition monitoring of HV equipment in electricity substations. A suggested band for radio PD detection is 0.3–1.5 GHz [1]. A low-cost, radiometric, PD wireless sensor network (WSN) has been proposed to provide real-time coverage for an entire substation [2]. The PD WSN is a collection of broadband radiometer sensors that measure PD activity interfaced to WirelessHART modules. The WirelessHART modules relay the PD activity data to an access point via wireless links. The access point is interfaced to a network and security manager and may also be interfaced to the network gateway. For such PD detection systems, the design of radiometer antennas is one of the major challenges.

Several antennas for PD detection have recently been reported [1,3–5]. These antennas, however, address multi-narrow-band operation [1,4] or achieve only modest VSWR performance (VSWR < 5) [3], or only work at higher frequency bands (0.75–1.5 GHz) and have no detailed specifications [5]. Wideband antennas, operating in the lower radio frequency (RF) band, include discone antennas, biconical antennas, log-periodic antennas, and spiral antennas. These antennas are larger, heavier, and more expensive than is practical for a dense PD wireless sensor network comprising many tens or even hundreds of radiometer sensor nodes. The design of radiometer antennas must meet some key requirements such as being light in weight, compact in size, and low

*Correspondence: y.zhang@hud.ac.uk

in manufacturing cost and allowing easy integration with a compact RF receiver. A novel simple structure broadband printed antenna meeting these requirements is presented here for PD detection applications. The compact antenna has satisfactory performance over the frequency band of 0.35 GHz to 1.38 GHz with small size of around $\lambda_s/4$ (where λ_s is the wavelength of the lowest frequency of the band, i.e. 0.35 GHz).

2. Radiated PD

PD comprises short-duration current pulses that occur predominantly in the first and third quadrants of the power system cycle. The frequency spectrum of the pulses has measurable energy extending well into the gigahertz region and a significant fraction of this energy is radiated from the conductors close to the PD source. Figure 1a shows a typical PD current pulse. The PD current pulse has short duration of the order of nanoseconds with a measureable energy spectrum extending up to several gigahertz. It is often approximated by a Gaussian waveform with half-amplitude width $T_l + T_h$ [4], given by:

$$I(t) = I_0 e^{-(t/t_0)^2}, \tag{1}$$

where $t_0 = (T_l + T_h)/2\sqrt{\log 2}$. The rise time T_l is usually less than the fall time T_h.

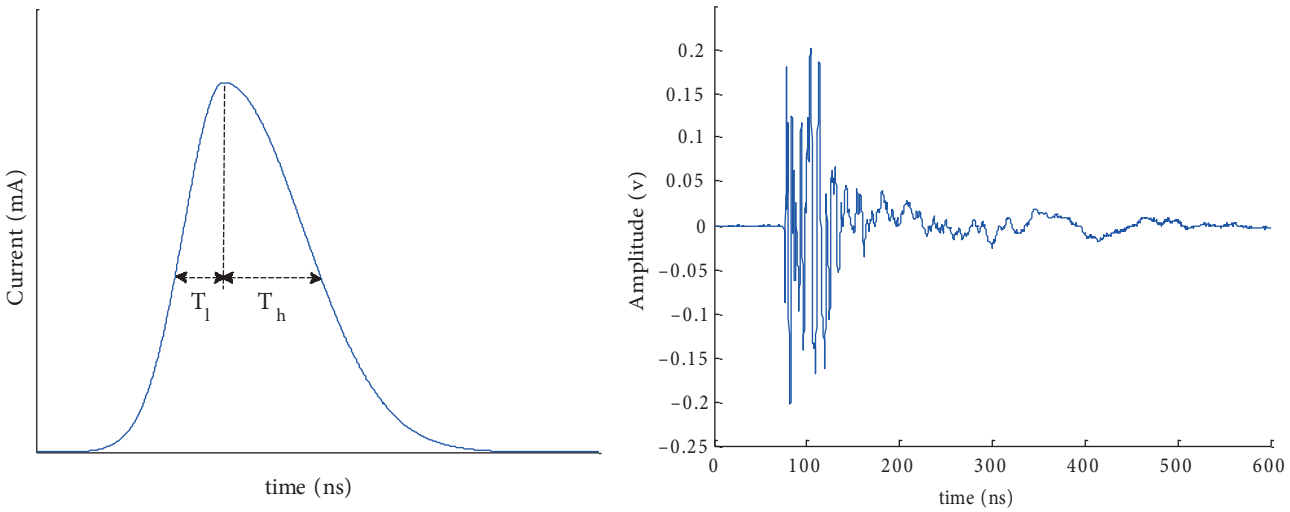

Figure 1. (a) Typical PD current pulse, (b) typical signal arising from radiated PD energy.

PD activity occurring inside a closed metallic chamber, e.g., the interior of an item of a gas insulated switchgear (GIS) or a transformer tank, results in a radiated signal that has been subject to multiple reflections. Electromagnetic signals radiated by PD current pulses have a time waveform and a frequency spectrum that depends on the impulse response of the radiating structure. Figure 1b shows a measured radiated signal. A cost-effective radiometric detection system is designed to measure the PD radiated signal. A compact broadband antenna is a key component of such a detection system. The designed antenna has successfully been applied to a radiometric WSN for PD detection and location, shown in Figure 2, with good performance.

3. Antenna design

The antenna has been constructed on FR4 substrate with thickness of 1.6 mm and dielectric constant of 4.9. The dimensions and constructed prototype are shown in Figure 3. It comprises a rectangular patch on one side

of the substrate and a ground plane on the other side. The patch is fed by a 50 Ω microstrip transmission line of width 3 mm (W_2).

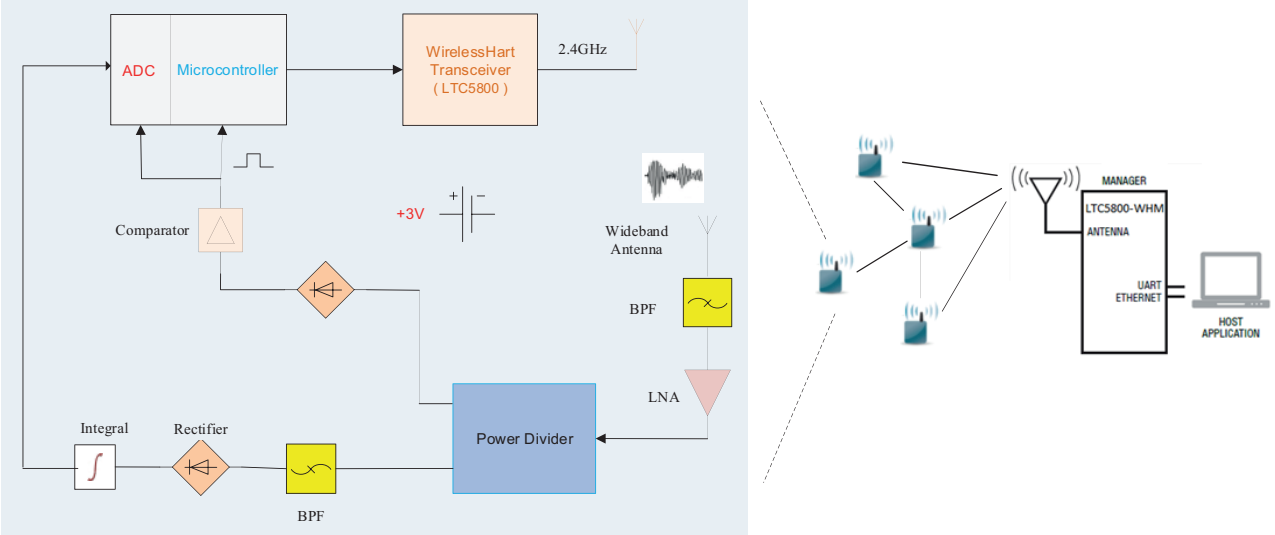

Figure 2. Radiometric wireless sensor network for PD detection and location.

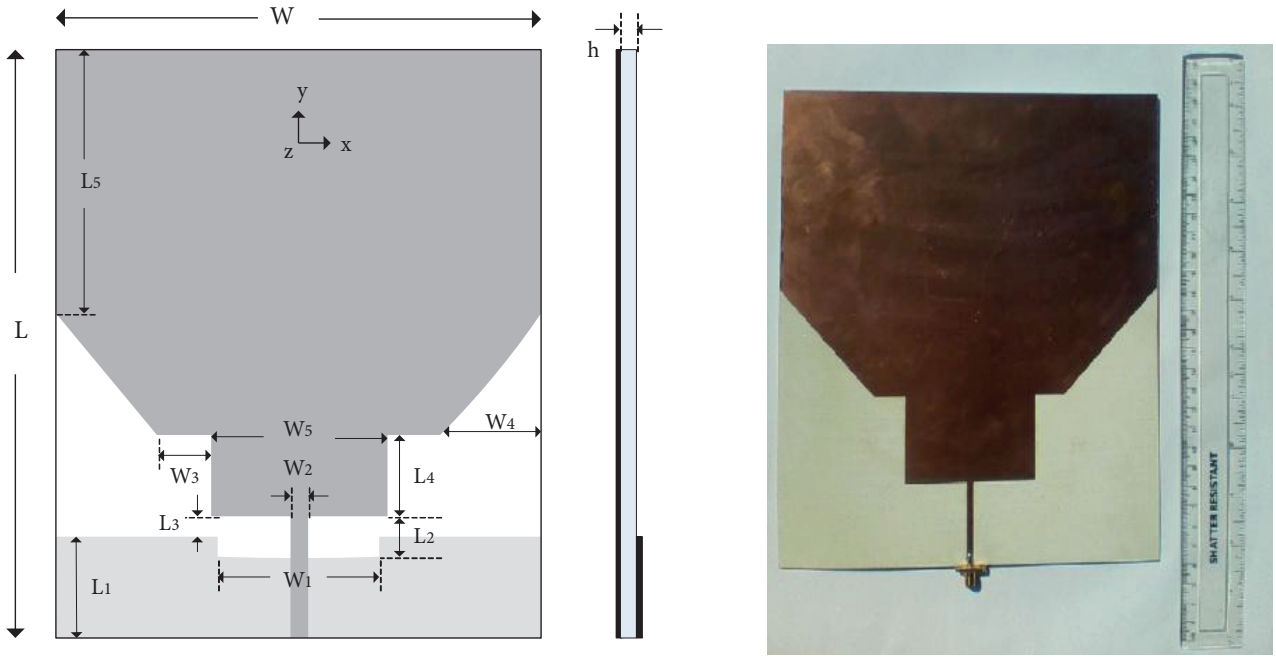

Figure 3. Antenna configuration and constructed prototype.

In most cases, the well-matched antenna is simply represented by a 50 Ω resistive load. For broadband antennas, the matching bandwidth can be achieved by overlapping several adjacent resonances, each of which can be represented by an RLC parallel circuit [6] as in Figure 4. A smooth transition between adjacent resonances ensures good impedance match over a broad frequency range.

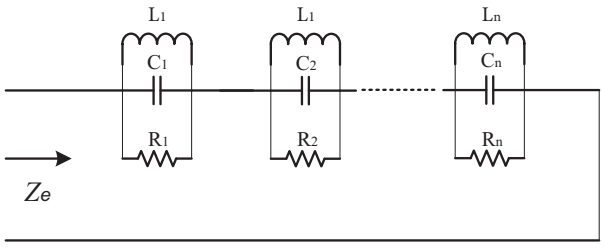

Figure 4. Equivalent circuit model of UWB antenna.

The monopole antenna and ground plane form an equivalent dipole antenna [7]. The simple structure antenna is compact (dimensions: 200 mm (W) × 240 mm (L)). The overall size of the antenna configuration is around $\lambda_s/4$ instead of $\lambda_s/2$ for the lower edge of the operating frequency. The low frequency limit is determined by the total effective length of the antenna current distribution, which includes the radiation patch and ground plane [8]. The frequency corresponding to the lower resonance of a rectangular planar monopole can be approximately given by:

$$f_r = \frac{144}{L + r_1 + r_2} GHz \tag{2}$$

$$\text{and } r_1 = \frac{A_g}{2\pi\sqrt{\varepsilon_{re}} L_1}, \tag{3}$$

$$r_2 = \frac{A_p}{2\pi\sqrt{\varepsilon_{re}}(L - L_1 - L_3)}, \tag{4}$$

where A_g and A_p are the area of the ground plane and the radiation patch, respectively. $\varepsilon_{re} = (1 + \varepsilon_r)/2$ is the effective dielectric constant of the composite dielectric. All dimensions are in millimeters. When the desirable frequency band of the antenna is available, the antenna size can be made compact by optimizing the area and structure of the ground and radiation patch.

Slots of dimensions $W_3 \times L_4$ are cut into the patch shoulders to electromagnetically couple the patch and ground plane. This significantly increases impedance bandwidth. The patch shoulders and bevels result in gradual variation of the distance from the patch to the ground plane. As a consequence, the impedance change from one resonance to another is small, ensuring good impedance match over a broad frequency range. Figure 5 shows the simulated return loss curves for different slot sizes L_4 when other parameters are kept unchanged. The gap L_3 between patch and ground plane introduces a coupling capacitance that further improves impedance matching over the broadband band [7–9]. The simulated return loss curves with different values of L_3 are plotted in Figure 6. The electromagnetic coupling between the lower edge of the patch and the ground plane can be properly controlled by adjusting L_3. The optimized gap distance is chosen as 2 mm. The leaky current between radiating patch and ground plant results in capacitive coupling. Larger gap L_3 leads to weaker coupling and therefore worse impedance matching. The ground plane is an integral part of the radiating configuration and its current distribution significantly affects the overall antenna characteristics. The rectangular notch in the ground plane improves both impedance matching and radiation characteristics at high frequency. Figures 7 and 8 show the simulated return loss for various values of W_1 and L_2 when L_3 is fixed at 2 mm. The simulated return loss curves with different values of W_3 are plotted in Figure 9, which shows that W_3 has a modest effect on antenna performance. Detailed investigation and extensive simulations have been undertaken with CST Microwave Studio to optimize the antenna structure and parameters: $L_1 = 40$ mm, $L_2 = 6$ mm, $L_3 = 2$

mm, L_4 = 43 mm, L_5 = 100 mm, W_1 = 64 mm, W_2 = 3 mm, W_3 = 16 mm, W_4 = 50 mm, W_5 = 68 mm, h = 1.6 mm.

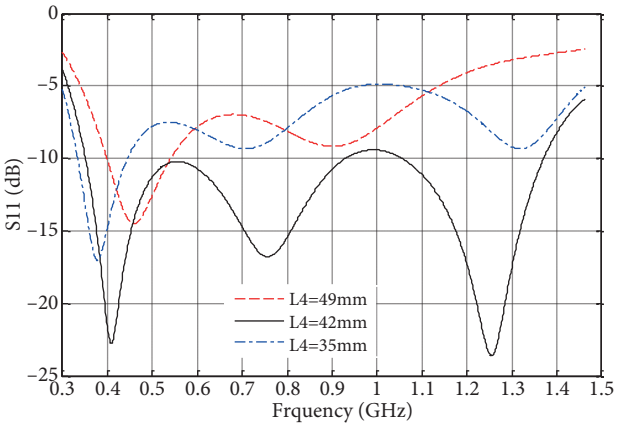

Figure 5. Simulated return loss for different L_4 values.

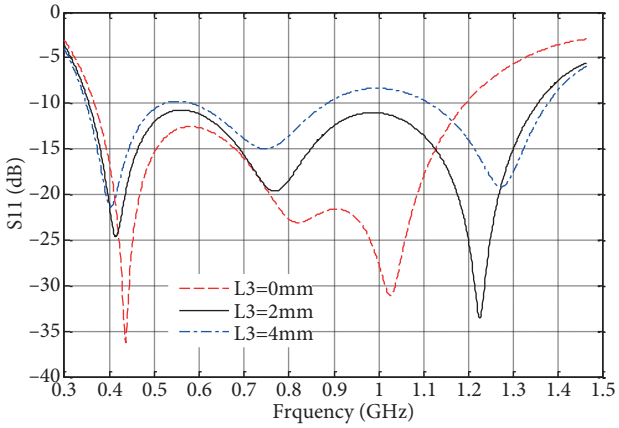

Figure 6. Simulated return loss for different L_3 values.

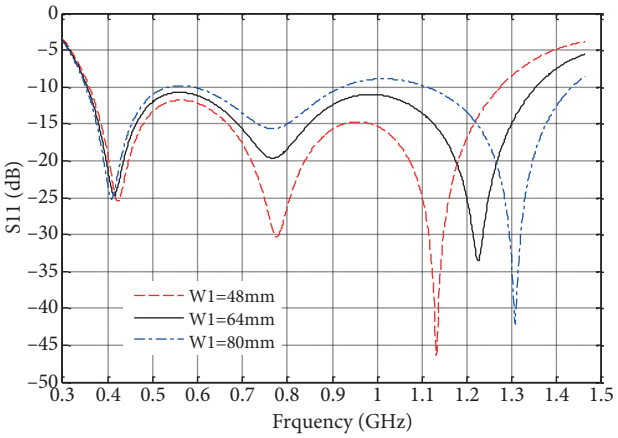

Figure 7. Simulated return loss for different W_1 values.

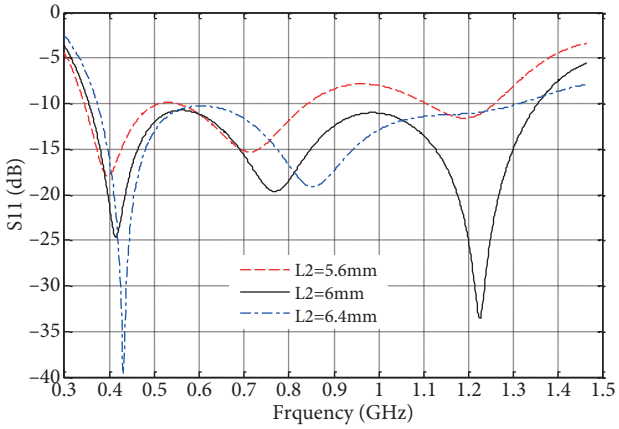

Figure 8. Simulated return loss for different L_2 values.

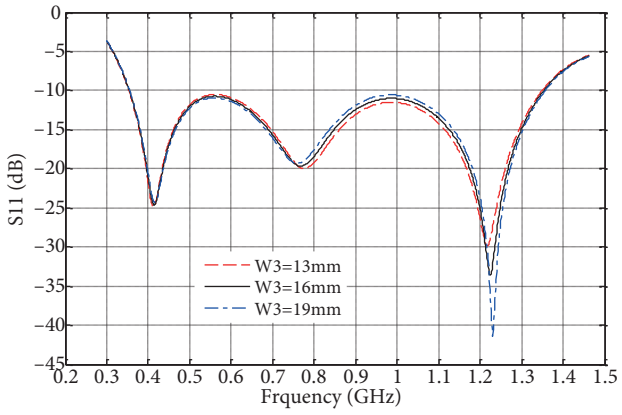

Figure 9. Simulated return loss for different W_3 values.

4. Results and discussion

The measurements were made in an anechoic chamber using a vector network analyzer. Figure 10 shows the measured and simulated return loss. The return loss (S11) –10 dB fractional bandwidth is 119% (from 0.35 to 1.38 GHz). The second resonance occurs at 0.77 GHz in the simulation but is not apparent in the measurement. This could be due to the effect of the SMA port. The normalized *yz*-plane (E-plane) and *xz*-plane (H-plane) radiation patterns have been simulated and measured at 0.45, 0.7, and 1 GHz (Figures 11–13). The *xz*-plane patterns are approximately omnidirectional over the operating frequency range. The *yz*-plane patterns have generally good symmetry. The symmetry becomes less good at the highest measurement frequency as the dimensions of the antenna become comparable to wave length. Overall, the radiation patterns of the antenna are very similar to those of a conventional monopole antenna. The simulated 3D radiation pattern is shown at 0.55 GHz as an example in Figure 14.

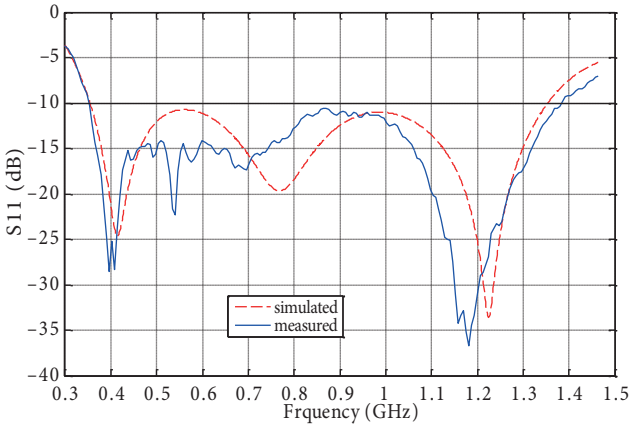

Figure 10. Simulated and measured return loss.

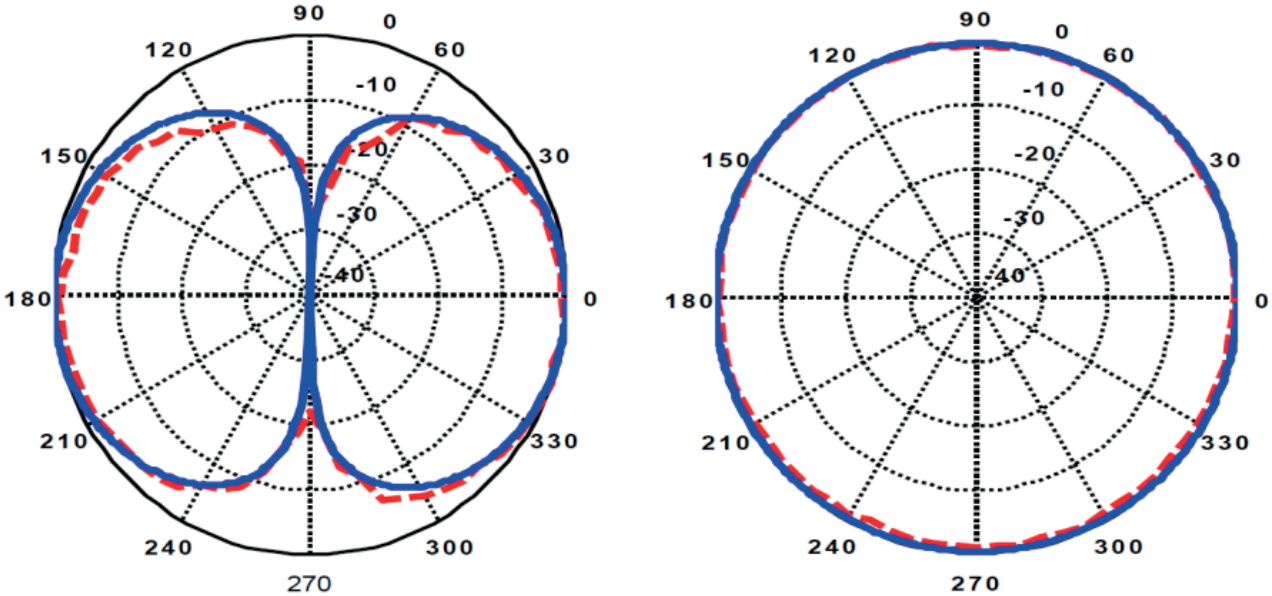

Figure 11. Simulated and measured radiation patterns in the *yz* and *xz* planes at 0.45 GHz. Solid lines denote simulations; dashed lines denote measurements.

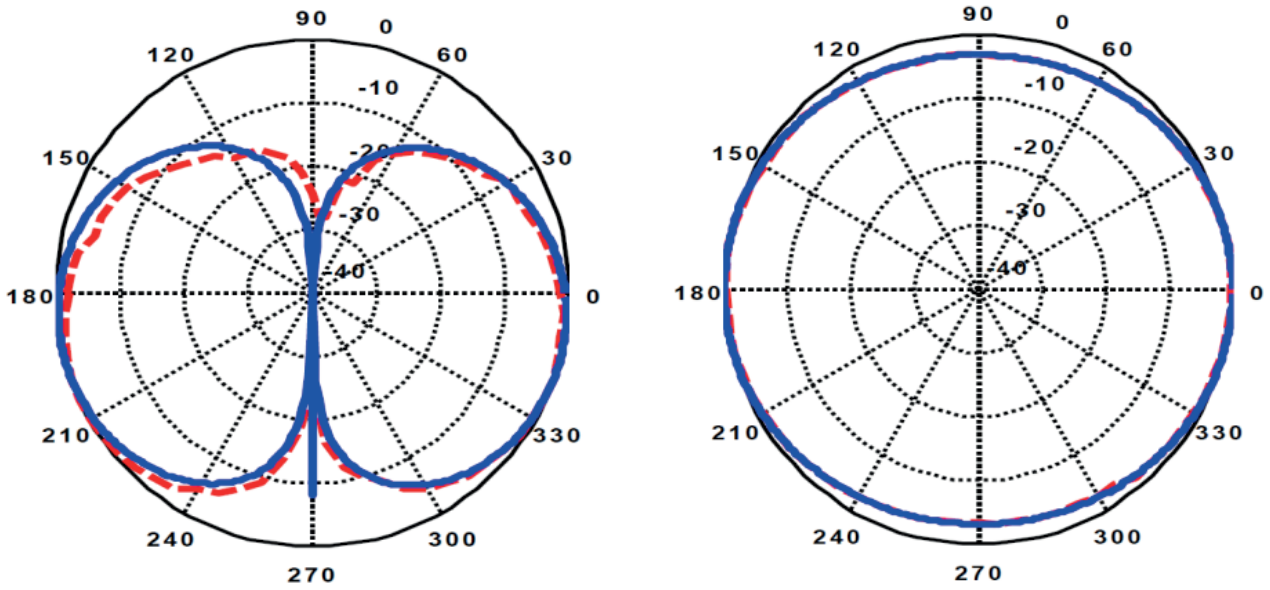

Figure 12. Simulated and measured radiation patterns in the yz and xz planes at 0.7 GHz. Solid lines denote simulations; dashed lines denote measurements.

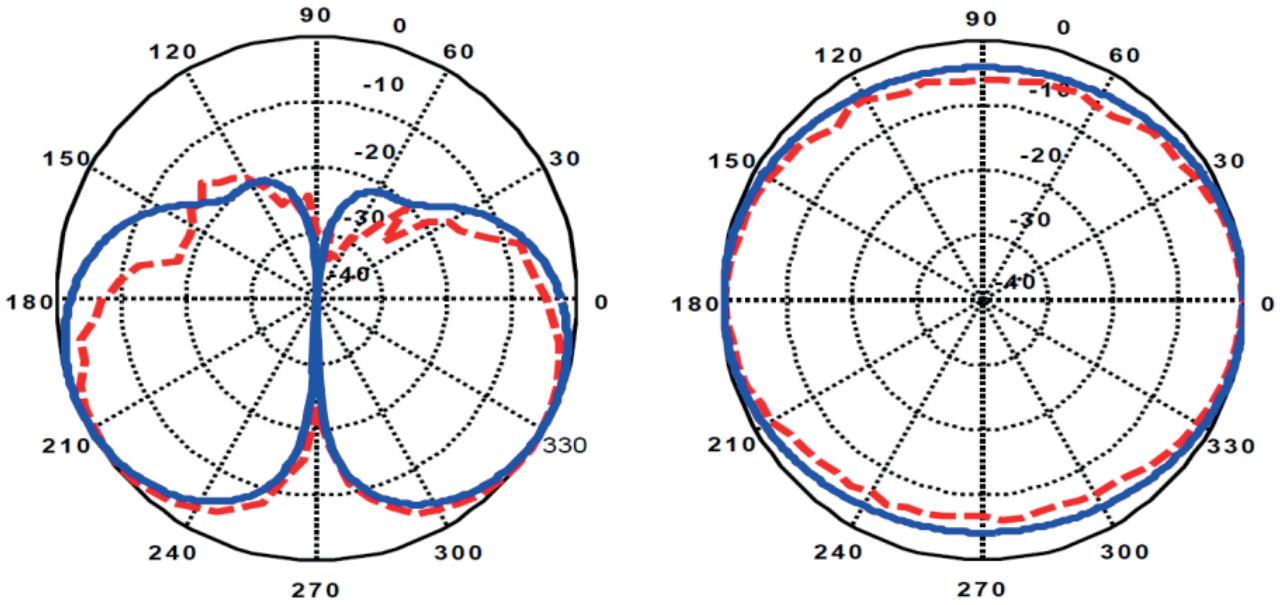

Figure 13. Simulated and measured radiation patterns in the yz and xz planes at 1 GHz. Solid lines denote simulations; dashed lines denote measurements.

The calculated variation of maximum gain with frequency is shown in Figure 15. The gain is 1.7 to 5.1 dBi over the design band. The figure indicates that the proposed antenna has good gain flatness with gain variation of less than 3.5 dBi throughout the entire frequency band. The gain decreases at a lower frequency band due to compact antenna size. Antenna gain is proportional to the effective radiation aperture. The antenna efficiency of the proposed antenna is equal to the radiation efficiency minus the return loss. The antenna efficiency has a maximum value of 93% and a minimum value of 54% within the frequency range of 0.35–1.38 GHz. The

average antenna efficiency is 81%. It is possible that information about the type and severity of insulation defect resides in the time series of received partial discharge pulses. If such information is to be extracted from the received signals then the shape of the pulses must be retained. This implies a linear phase (constant group delay) antenna since such an antenna (assuming constant gain across its passband) will not significantly distort the received signal. In this case pulse dispersion must be minimized and group delay will be important. Figure 15 presents the simulated group delay, which varies by less than 2 ns from its mean value over most of the operating frequency band. This means that the broadband antennas have good transient response in the working band. The Table shows the comparison between the proposed antenna and other reported antennas for PD detection.

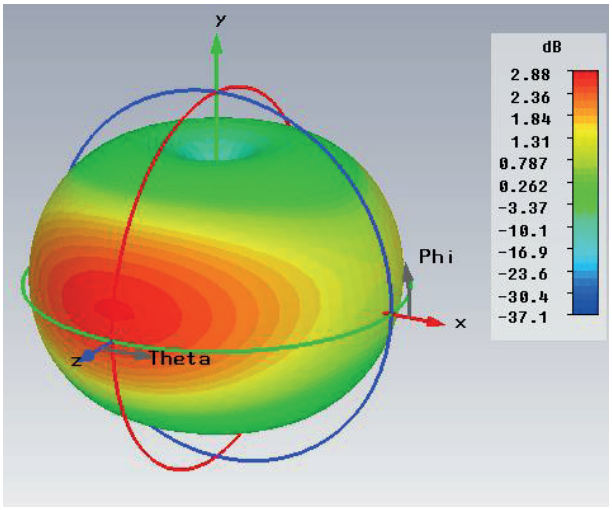

Figure 14. Simulated 3D radiation pattern at 0.55 GHz.

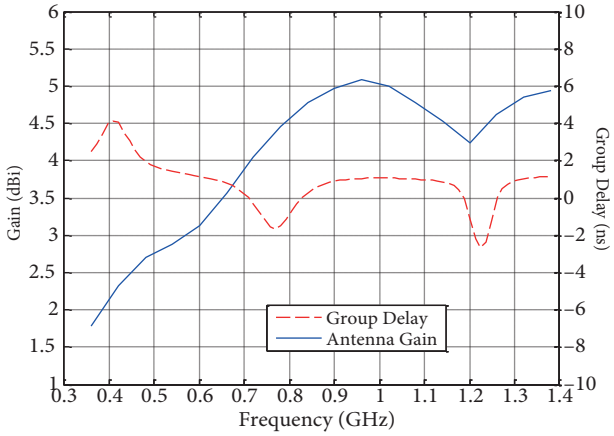

Figure 15. Antenna gain and group delay.

Table. Performance comparison of various antennas.

Antennas/parameters	Bandwidth (MHz)	VSWR	Dimensions (cm)
The proposed antenna	350–1380	< 2	24×20
Antenna in reference [1]	480–520	< 2	19.12 (diameter)
	800–850		
	1100–1200		
Antenna in reference [3]	339–375	< 5	7×7
	395–440		
	450–1000		
Antenna in reference [4]	1800 narrowband	< 2	4.19×2.94

5. Conclusion

A compact microstrip-fed planar broadband antenna for PD detection applications has been presented. The antenna satisfies a –10 dB return loss requirement from 0.35 to 1.38 GHz. The radiation pattern is close to that of a simple monopole. Predicted variation in group delay is not more than 2 ns. The proposed broadband antenna provides wider impedance bandwidth than the single or multiple narrowband antennas in [1,4] and the Hilbert antenna (VSWR < 5) in [3] to collect more PD energy for higher radiometric sensitivity. The antenna is compact, light, and inexpensive to manufacture, making it suitable for use in a dense sensor network.

Acknowledgment

This work was supported by the U.K. Engineering & Physical Sciences Research Council (EPSRC) under grant EP/J015873.

References

[1] Ye H, Qian Y, Dong Y, Sheng G, Jiang X. Development of multi-band ultra-high-frequency sensor for partial discharge monitoring based on the meandering technique. IET Sci Meas Technol 2014; 8: 327-335.

[2] Zhang Y, Upton D, Jaber A, Ahmed H, Saeed B, Mather P, Lazaridis P, Mopty A, Tachtatzis C, Atkinson R et al. Radiometric wireless sensor network monitoring of partial discharge sources in electrical substations. Int J Distrib Sens N 2015; 2015: 438302.

[3] Li J, Wang P, Jiang T, Bao L, He Z. UHF stacked Hilbert antenna array for partial discharge detection. IEEE T Antenn Propag 2013; 61: 5798-5801.

[4] Shibuya Y, Matsumoto S, Konno T. Electromagnetic waves from partial discharges in windings and their detection by patch antenna. IEEE T Dielect El In 2011; 18: 2013-2023.

[5] Lopez-Roldan J, Tang T, Gaskin M. Optimisation of a sensor for onsite detection of partial discharges in power transformers by the UHF method. IEEE T Dielect El In 2008; 15: 1634-1639.

[6] Pele I, Chousseaud A, Toutain S. Simultaneous modeling of impedance and radiation pattern antenna for UWB pulse modulation. In: IEEE 2004 Antennas and Propagation Society International Symposium; 20–25 June 2004; Monterey, CA, USA. New York, NY, USA: IEEE. pp. 1871-1874.

[7] Jiang W, Che W. A novel UWB antenna with dual notched bands for WiMAX and WLAN applications. IEEE Antenn Wirel Propag Lett 2012; 11: 293-296.

[8] Thomas KG, Sreenivasan M. A simple ultrawideband planar rectangular printed antenna with band dispensation. IEEE T Antenn Propag 2010; 58: 27-34.

[9] Hong C, Ling C, Tarn I, Chung S. Design of a planar ultrawideband antenna with a new band-notch structure. IEEE T Antenn Propag 2007, 55: 3391-3397.